FACULTY OF SCIENCE
UNIVERSITY OF COPENHAGEN

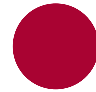

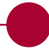

Merlin von Soosten

Characterization of InAs nanowires strained by AFM manipulation

Bachelor Thesis in Nanoscience

Supervisor:
Thomas Sand Jespersen

March 15, 2013

Characterization of InAs nanowires strained by AFM manipulation
Bachelor Thesis in Nanoscience

Written by
Merlin von Soosten

Center for Quantum Devices
Niels Bohr Institute
Faculty of Science
University of Copenhagen
Universitetsparken 5
2100 Copenhagen E
Denmark

http://qdev.nbi.ku.dk

In this thesis I present a characterization of strained Indium Arsenide nanowires. Aiming for the greates curvature possible, a concise method has been developed to induce strain in the crystal structure by bending single nanowires using an AFM. Bended nanowires were characterized by high resolution transmission electron microscopy, verifying a non invasive bending procedure. Knowledge was gained on characterization of strained nanowires by Raman spectroscopy. And finally a bended wire was contacted to enable for low temperature electron transport measurements.

Table of Contents

Introduction **1**
1 Characterization Techniques **2**
1.1 Atomic Force Microscopy 2
1.1.1 Introduction to Atomic Force Microscopy. 2
1.1.2 Principle of the Atomic Force Microscope 2
1.2 Transmission Electron Microscopy 3
1.2.1 Introduction to Transmission Electron Microscopy. 3
1.2.2 Principle of a Transmission Electron Microscope 3
1.3 Raman Spectroscopy 4
1.3.1 Introduction to Raman Spectroscopy 4
1.3.2 Setup 5
2 Experiments **7**
2.1 Sample Preparation 7
2.2 Bending Nanowires 8
2.2.1 Introduction to Nanowire Bending 8
2.2.2 Optimizaton of the Bending Technique 9
2.2.3 Detailed Examples of Bended Wires. 11
2.2.4 The Quick and Dirty Option 13
2.3 Strain and Defect Analysis using TEM 13
2.3.1 Characterization by regular TEM 13
2.3.2 HRTEM characterization at Risø. 16
2.4 Raman Spectroscopy 16
2.4.1 Spectra along Bended Nanowires 16
2.4.2 Mapped Raman Spectra 18
2.4.3 Possible Setup Improvements 20
2.5 Device Fabrication for Electron Transport Measurements 21
2.6 First Electron Transport Measurements 23
3 Conclusion and Outlook **24**
3.1 Conclusion. 24
3.2 Outlook 24
Acknowledgements **25**
Bibliography **26**

Appendix **27**
A Bending Nanoowires using an Atomic Force Microsope **28**
B High Resolution TEM Images **31**

Introduction

This thesis summarizes the work performed for my bachelors project. The main focus of this experimental work is based on controlled nanomanipulation of semiconductor nanowires (NWs). Several tools for nanoscale characterization have been applied to gain new knowledge on Indium Arsenide nanowires, these cover atomic force microscopy (AFM), transmission electron microscopy (TEM) and Raman spectroscopy.

Nanoscale semiconductors gained great attention in fundamental research, due to their special electrical and optical properties. NWs are part of this vast field in natural sciences, expected to solve many challenging problems and open new possibilities, e.g. pathways to sustainable energy and eficcient computing. Due to their small size, semiconductor NWs do not behave as bulk samples of the same material. Furthermore, due to their geometry, they are often referred as one dimensional systems; the lengths of NWs often exceed their witdh by several orders of magnitude. This makes them especially interesting for electronic components, ranging from solar cells over nanoscale sensors in biology to quantum computers[1][2][3].

Semiconductor nanowires can be fabricated from many different materials, ranging from group IV elements, such as Si/Ge, to group III/V and even further to group II/VI combinations. Here pure, single-crystal Indium-Arsenide nanowires are studied, grown in the $\langle 111 \rangle$ direction by molecular beam epitaxy[4]. A small effective electron mass and thus high mobility, described by the band structure, makes this semiconductor a great candidate for studies on electron transport and spin-orbit interactions. In the last few years, scientists have investigated InAs NWs and many electronic devices were fabricated to study fundamental semiconductor characteristics, spin-orbit interactions and spin coherence[3].

Decent control and measurement of the electron spin are nessecary ingredients for quantum devices. It has been proposed that quantum dots defined in bended carbon-nanotubes allow for controlled spin manipulation[5]. In general, strain induced to semiconductors is known to affect the band structure and thus fundamental parameters such as spin-orbit coupling[6] are altered.

In this study, InAs nanowires are investigated, focused on the experimental work, an optimized procedure is established to reproduceably bend NWs with an AFM. Verification of the induced strain is perfomed by high resolution TEM. It was shown by Chen et al.[7] that Raman spectroscopy can be used to effectivly study strain induced in InP NWs. Thus, this study also aims at incorporation of Raman spectroscopy as a fast and non destructive characterization tool for strained nanowires.

1 Characterization Techniques

1.1 Atomic Force Microscopy

1.1.1 Introduction to Atomic Force Microscopy

The Atomic Force Microscope (AFM) is a strong tool to visualize and manipulate surfaces of different materials on atomic resolutions. This section describes the principle of atomic force microscopy and how it was applied in this study.

1.1.2 Principle of the Atomic Force Microscope

Surface visualization with an AFM is usually done using one of the main characterization techniques, namely contact- and tapping-mode. These two techniques differ greatly in principle while both of them reveal detailed information about the surface structure. In general the contact mode is known for its accuracy and is used to achive true atomic resolution while the tapping mode is suitable for fast analysis as well as non destructive measurements.

Contact Mode. In contact mode the AFM-tip is kept at a constant distance to the surface. Due to the interaction forces between the tip and the surface, namely Van der Waals and electrostatic forces, the cantilever will be deflected when the surface-tip distance changes during horizontal tip movement. The deflection is translated into vertical tip movement to obtain the desired interaction force. The movement of the tip is measured and reveals the surface profile. Due to the continous surface contact, tip movement might be destructive, which usually not is a problem when scanning in tapping mode.

Tapping Mode. In tapping mode the cantiliever is continously oscillating just below or above its resonance frequency. The cantilievers used had a resonance frequency around 320 kHz and a force constant of 40 N/m. When the tip is moved closer to the surface, at some point it will touch it and thereby reduce the oscillation frequency due to the energy transfer to the sample. The oscillation frequency is kept constant by a feedback loop controlling the piezo oscillating the tip. Also, the oscillation amplitude (which is measured by the laser deflection) will decrease when the tip hits a bump on the surface, or it will be increased where the tip hits a valley. The measured amplitude, along with other parameters, controls the vertical movement of the head to maintain the desired amplitude.

The strong benefit of this mode is the low surface interaction, the tip will only touch the surface at the measuring points and it will only do so in the vertical direction, which

reduces potential surface distruction.

Surface Manipulation. The use of an AFM is not limited to visualize a surface but can be extended to manipulate it. Surface manipulation can be done using a variety of techniques which will attain just as many different results. To name a few techniques; nano particle positioning for device fabrication and dissection of biologic tissues span very different disciplines[8][9].

For this study it was essential to bend nanowires deposited on different surfaces. As described elsewhere [10] it is possible to do so by pushing the nanowires along the surface with the AFM tip which also is used for scanning. This allows for nanowire visualization and manipulation with the same setup.

1.2 Transmission Electron Microscopy

1.2.1 Introduction to Transmission Electron Microscopy

Transmission electron microscopes (TEMs) are used to study structures smaller than the resolution limit of optical microscopes (theoretically around 0.2 µm). The resolution of an optical microscope (OM) is limited by diffraction, which is dependent on the wavelength of the transmitted light. Optical microscopes use light in the visible and near visible range, while in TEMs, electrons are transmitted through the specimen. Electrons behave as waves with a much smaller wavelength than visible light, thus they can be used to study smaller structures. In a TEM electrons have wavelengths in the oder of pm. Thus theoretically the resolution of a TEM is much smaller than single atoms, which in practice is limited due to the imperfect electron beam.

1.2.2 Principle of a Transmission Electron Microscope

In general, a TEM is comparable to an OM, both setups (fig.1.1a) contain a radiation source which is focused on the specimen by lenses and a magnified image can be seen directly (OM) or on a phosphorous screen (TEM) and in both cases a CCD camera can be used to record a digital image. The difference in the setups lies in the lenses which are made of refractive materials in case of the OM, while electromagnetic coils focus or deflect the electron beam in a TEM. Also an OM can be used in ambient atmosphere while in a TEM a vacuum chamber is required due to interactions of electron with the atmosphere.

While diffraction limits the resolution of an OM it is excessively used in transmission electron microscopy. Electrons are diffracted by atomic planes in crystal structures which allows direct studies of the reciprocal lattice (diffraction mode). When Braggs law[1] is fullfilled constructive and destructive interference of scattered waves creates a

[1] Braggs law: 2d $\sin(\phi) = n\lambda$ where d is the lattice spacing, ϕ the incident wave angle, n an integer and $\lambda$the wavelengt of the electron.

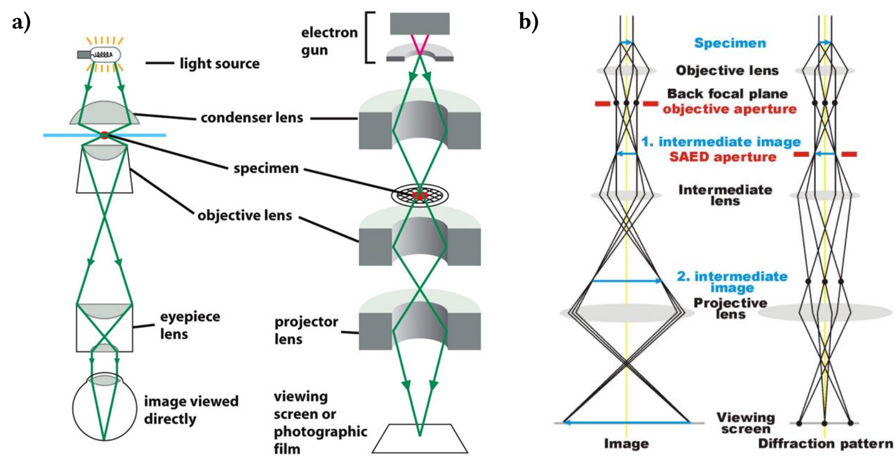

Figure 1.1. Principle of a transmission electron microscope. **a)** Comparison of a TEM to an optical Microscope.[11] **b)** Comparison between direct imaging and imaging of the diffraction pattern.[12]

diffraction pattern, which is the two dimensional representation of the reciprocal space (fig.1.1b).

In a regular TEM only electrons passing directly through the sample without scattering *or* only scattered electrons are used for imaging (i.e. Bright field and Dark field configurations). High resolution TEM (HRTEM) uses both configurations simultaneously. In this case contrast arises form constructive and destructive interference of the direct and the scattered electrons, which allows for atomic resolution.

1.3 Raman Spectroscopy

Raman spectroscopy is a versatile tool used in many desciplines to identify and characterize materials and their composition.

1.3.1 Introduction to Raman Spectroscopy

Raman scattering refers to light scattered inelastically by optical phonons in solids or molecular vibrations. When a photon is absorbed by a compound, the photon energy is transferred which leaves the compound it in an excited virtual energy level. There are basically two pathways for relaxation; 1. the compound relaxes back to its ground state, emitting a photon with the same energy as the absorbed photon (Rayleigh scattering). 2. The compound ralaxes to an energy level of an excited (vibrational) state, emitting a photon with a lower energy (Stokes scattering). Also a compound can absorb a photon while it is in an excited state, relaxation can happen to a groundstate and therby a photon of higher energy is emitted (Anti-Stokes scattering). Thus the reflected light

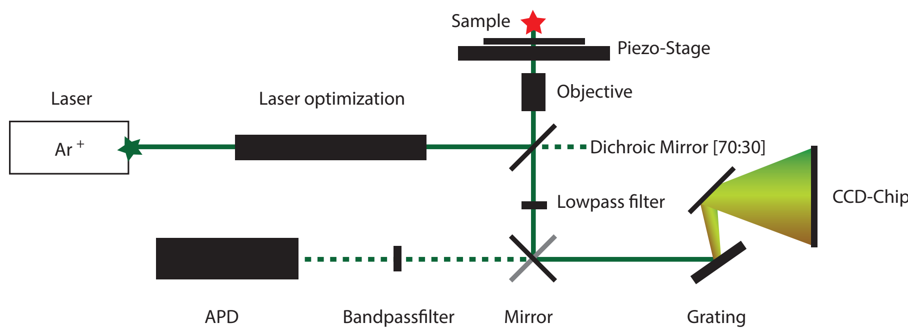

Figure 1.2. Simplified schematic of the setup which was used for Raman spectroscopy.

(Raman signal) of a compound is dependent on the vibrational modes available.

Raman Spectroscopy refers to the analysis of vibrational modes by measuring the Raman signal, usually only the Stokes signal is measured. This is due to the Rayleigh signal not changing in energy while the anti-Stokes signal is higly temperature dependent. In goup III-IV Semiconductor alloys such as InAs usually two vibrational modes are available, called Transversal and Longitudinal Optical modes (TO and LO). In Raman spectroscopy Lasers are used for a discrete photon energy excitations.

Vibrational energies are dependent on the strength of chemical bonds, thus a raman spectra acts as a fingerprint for identifying compounds. Here the InAs nanowires are studied and the composition is well known. A change of the crystal structure affects the energies of vibrational modes due to the changed interatomic potential. Thus Raman spectroscopy can also be used to measure strain in crystals.[13]

In this study Raman spectroscopy was applied, on nanowires, to evaluate changes of the vibrational modes in comparison to the strain induced by the bending with an AFM.

1.3.2 Setup

The setup used for Raman spectroscopy was build in the lab of Tom Vosch[2], basically it consists of a Laser, an invertet confocal microscope and the possibility to measure the Raman signal by an Avalanche Photo Detector (APD) or by a spectrometer.

The simplified setup is shown in figure 1.2. An Argon ion laser emits light of discrete wavelengths, one of them is at 514.5 nm which is selected in the setup used. The laser-light is optimized with different filters and apertures, this generates a highly homogenous laser beam. In the setup an inverted confocal microscope is used to focus the beam on the sample. Due to this configuration the excitation and emission light passes through the objective on the same path. Thus a dichroic mirror, which reflects 30 % and transmits 70 % of the light, is used. A lowpass filter then only allows light with

[2]Tom Vosch Group, Nano-Science Center, University of Copenhagen.

wavelengths above 517 nm, reflected from the sample, to pass further. For detection of the Raman signal a spectrometer or the APD is used. The spectrometer uses a grating to refract the emitted light into a spectrum which then is recorded on a CCD-Chip. If the APD is used the reflected beam passes throug an other filter. Here a bandpass filter is used, in combination with the lowpass filter only a small range of the spectrum emitted by the sample is detected by the APD. Inferring from the setup using a high quality oil immersion objective with a numerical aperture (NA) of 1.2 and the definition of resolution; $R = {}^{0.61 \cdot \lambda}/_{NA}$, the laser spot size is expected to lie between $250 - 300$ nm at the focused sample.

When the spectrometer is used, calibration of the spectra is nessecary, a CCD-Background image (no Raman signal) is recorded and removed from the recorded spectra. Also all Raman spectra shown in this report are calibrated to a Toulene reference spectra with known Raman peaks.

2 Experiments

2.1 Sample Preparation

Manipulation of nanoscale structures, i.e. single nanowires, requires detailed knowledge of their position, to allow the use of different manipulation or visualization techniques. Here SEM and TEM measurements, AFM manipulation as well as high precision lithography was applied.

The usual way to achieve detailed information of position is to deposit the nanoscale structures on a surface with a known pattern which is visible in microscopes and can be used for lithography alignment. In this study highly doped silicon substrates, covered with a 500 nm insulating SiO_2 layer were used. The substrates were prepared with a pattern by Anders Jellinggaard[3] and Nino Ziino[3]. The ready to use chips included bonding pads, alignment marks and an array of $196 \cdot (100\,\mu\text{m})^2$ individually distinguishable 'fields'. Also a software to automatically align optical images in a DesignCAD file was provided. The pattern (fig. 2.1) was created by e-beam lithograpy and deposition of $5/100$ nm Ti/Au as described in detail in section 2.5.

Nanowires used here were grown, using molecular beam epitaxy[4], by Morten Hannibal Madsen[3] in 2010, with the batch number *NBI 591.* The NWs consist of InAs with a diameter around 70 nm and lengths rannging from 6 to 11 µm [14]. To deposit NWs on a substrate, different techniques can be used. Here a small piece of the NW-forest was suspended in Isopropyl Alcohol (IPA) and by appyling ultrasound to the solution the NWs break from the substrate and dissolve. A droplet of the solution was then applied to the patterned substrates and finally air-drying leaves the NWs randomly distributed on the surface.

Inspection of the deposition process was done using an ordinary optical microscope in bright- and dark-field settings, where the majority of the NWs are visible. Images were taken on alignment fields containing long straight wires with free space surrounding them, through automated image positioning in the template CAD file. NW-maps of the respective chips were created and later used to identify single NWs. Figure 2.1 shows such a pattern with positioned optical images. A zoom of one alignment field shows an inverted dark field image with a single NW which was later bended with great success. Also shown are alignment marks and an binary identification pattern, used in the automated image positioning process, as well as a readable identification number.

Nanowires were also bended directly on TEM grids to analyze them for defects and strain due to the manipulation of the wire, which is described in section 2.3. For this purpose nanowires were deposited on three different TEM grids, two grids with Silicon-

[3] Center for Quantum Devices, Niels Bohr Institute, University of Copenhagen

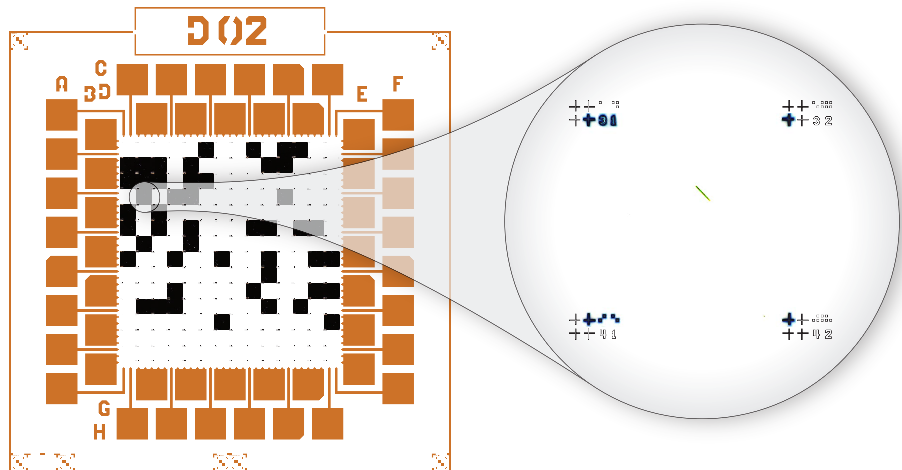

Figure 2.1. Design of a pattern used on the samples in this study. Optical images are automatically aligned and placed in the schematic. The magnified image shows a field on the pattern with identification and an (inverted) image of a nanowire.

Nitride membranes of 15 and 50 nm thickness and one grid with a 40 nm SiO_2 membrane, all membranes were supported by solid silicon. An array of nine $(100\,\mu m)^2$ windows of suspended membrane were available on the Si_3N_4 grids while the SiO_2 grid had an array of 24 windows of $(100\,\mu m)^2$.

2.2 Bending Nanowires

2.2.1 Introduction to Nanowire Bending

During this study more than 80 nanowires were bended which allowed for an optimization of the NW-bending technique, based on nanowires deposited on a SiO_2 surface using patterned chips as described above.

Bending nanowires is done following a simple procedure: 1. Scan the surface in tapping mode to locate the wire. 2. Disable feedback and position the tip close to the surface beside the wire. 3. Move the tip horizontally to push the wire along the surface. 4. Enable feedback and rescan the surface.

To study the influence of the induced strain it is desireable to obtain a bend with a large curvature without inducing defects. Naturally all measurements on bended wires will have to be compared to straight wires at the same conditions. This is effectively done by leaving a part of the wire untouched. For electrical measurements the wires have to be contacted on a straight and a bended part, which is described in more detail in section 2.5.

These criteria and requirements lead to an optimal bend position x_{bend} at 2 µm from

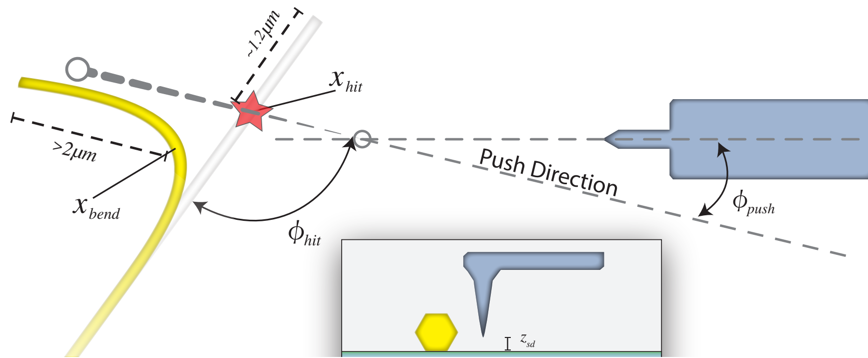

Figure 2.2. Schematic of the nanowire bending process by AFM manipulation. The relation of optimized parameters for successful bending are shown.

one end of a wire with a length of 9 µm and above.

Furthermore, nanowires were bended on Si_3N_4 and SiO_2 membranes (TEM grids) to allow for analysis using electron microscopy. Due to the different surface interaction, betweeen wire and membrane compared to the SiO_2 wafer, bending behaved differently. In general the bending radius was larger which is a result of lower attraction of the wire to the surface, which enabled moving entire wires along the surface. The 50 nm Si_3N_4 membrane provided good support during bending, while the 15 nm membrane was unusable. The membrane oscillated below the AFM tip even when applying gentle forces by tuning the parameters for scanning frequency, amplitude setpoint, intregal and proportional gain. Membrane oscillation was also observed on the SiO_2 grid but wires could still be bended. In both cases membrane vibrations were visible in the optical microscope at the AFM.

2.2.2 Optimizaton of the Bending Technique

There are a few parameters which influence the result of the bending process, so they were optimized to obtain the desired bended nanowires. The important parameters include: 1. Hit position (x_{hit}), 2. Hit angle (ϕ_{hit}) and 3. *x*-*y* velocity during bending. However, during the bending process it has been observed that other parameters could have great impact on the result: 4. Tip-surface distance (z_{sd}) during *x*-*y* move. 5. push direction to tip holder orientation $\left(\phi_{push}\right)$. The parameters and their effects are described in detail below and illustrated in figure 2.2.

1. The hit position (x_{hit}) accounts for the placement of the bend, if it is too close to the end of a NW ($x_{hit} < 0.7\,\mu\text{m}$) only a little part of the wire will be bended which makes it unusuable for electrical contacts. If it is too far away from the end the surface adhesion is too strong so the wire will be cut or the tip will break. Best

results in terms of the distance from the bend to the end of the NW were achieved at a hit position $x_{hit} \approx 1.2$ µm from the end of the wire.

2. The hit angle (ϕ_{hit}) mainly accounts for the curvature of the bend, a smaller hit angle increases the chance of successful bending, but also limits the achievable curvature. Several repeated small angle bends will result in larger curvatures as well but this is time consuming due to several full image scans to verify the NW position and repeated slow motion moves while pushing to the NW. 'Blind bending' (bending repeatedly without rescans) saves some time but involves uncontrolled manipulation and a poor hit/miss ratio. Also, repeatedly hitting the wire with the AFM-tip might reduce sample quality.
   Bending with a 90 ° hit angle showed good results at a great success rate. To increase curvature even further a larger angle is required which increases the chance of breaking the NW. The best results were obtained with a hit angle around 110 °.
3. When moving the AFM-tip in the *x-y* direction, the momentum at the impact on the NW increases with the tip velocity, thus a larger *x-y* velocity increases the force acting upon the NW which could induce small defects or larger damage to the NW or the tip. During the experiments the tip velocity ranged from 0.01 µm/s to 2 µm/s. At 1-2 µm/s the NW was literally cut or the AFM-tip was broken. As expected, the best results were observed at 0.01 µm/s which is the lower limit of the AFM system.
   The AFM tip type used during the bending process had a tip size with a radius less than 10 nm which is great for probing nm sized objects but might not be well suited for bending NW's. A larger tip would have a larger impact surface which would distribute the force on the NW and reduce stress on the tip as well. Thus the tip velocity could be increased.
4. When turning feedback off during scan, the tip will be positioned at a rest position, which roughly lies at the center of the scanning amplitude. Thus the effective tip-surface distance (z_{sd}) was never known during manipulation and the optimal z-movement before bending had to be found experimentally. If the tip-surface distance is too large, the wire will not be hit or just scratched. If the tip is moved too far down it may be in direct contact to the surface.
   Scratching the wire with the sharpest point of the tip, or pushing it into the surface before moving horizontally, usually breaks the tip.
   Nevertheless, it seems that the rest position does not change a lot and as a rule of thumb a z-movement of 50 nm closer to the surface was found to yield good results.
5. It was not concidered in the first place but the push direction to tip holder orientation (ϕ_{push}) could affect the probability of success. Independent of the scanning direction the NW had to be pushed or pulled roughly in the direction of the tip. In some cases physically pushing sideways did not bend the wire but moved the tip in the tip holder which was seen as an entire image shift of a several microns after a rescan. This is a construction issue as the tip is only held in place by a metal clip.

2.2.3 Detailed Examples of Bended Wires

The parameters above define an optimal situation and were found during several attempts to bend NWs. Although following these guidelines does increase the probability of success to bend a NW with a single movement, it is not a standard situation. Thus in most cases a twofold bending process had to be undertaken to achieve a great bend i.e. $\phi_{bend} > 90\,^{\circ}$.

In this section some examples are described to illustrate the bending process. Only final images are shwown here, initial and intermediate steps are summarized in Appendix A. The first six examples show nanowires on SiO_2 wafers and the last two are examples of NWs bended on Si_4N_3 TEM-grids.

Cutting a Nanowire. This first example shows a NW, cut with the AFM tip due to fast x-y movement. Figure 2.3a shows the NW after cutting with a tip velocity of 2 µm/s. Note that the final scan does not show a junk left from the tip, thus the tip is still intact and is not destroyed during fast cutting.

Bending a Nanowire. A typical single-movement bend is shown in figure 2.3b, here a tip velocity of 0.01 µm/s and a the hit angle of $\phi_{hit} \approx 90\,^{\circ}$ was applyed. During bending the tip was lowered by 45 nm from its rest position. Figure 2.3b shows the bended wire with an angle of 75 ° but also the original position of the wire on the substrate, as well as the tip movement path. The latter has been observed on some samples, and could be a consequence of condensed water and other gases from the ambient atmosphere.

Flexible Nanowires. During the studies there was a single nanowire (on SiO_2 substrate) which showed an enormous flexibility. Figure A.3b shows the wire after two bending moves from the lower right corner, 2.3c shows the final scan after a third move which was in parallel to the initial direction of the wire.

One might argue that the structure is not a NW, the parameters (height = 80 nm, lenght = 6.6 µm) however compare well to the other nanowires, also wires on Silicon Notride membranes showed increased flexibility due to decreased surface interactions.

Strong Strain in the Crystal Structure - Snap Back. Presuming the substrate was covered with a aquaeous layer as mentioned earlier, moving NWs accumulates water on the side of the wire while pushing it along the surface. This is usable to identify an intermediate NW position (i.e. the most bended configuration) between two full image scans.

An extreme example of relaxation of a NW is summarized in figure A.4. An initial bend left the NW virtually untouched but there is evidence for a sucessful bend; the trace of collected surface condensate as well as broken tip pieces in figure 2.3d tell the story of a bended wire. Using the same parameters for a second bend resulted in a bend close to the initial bend (fig.A.4c), where a broken piece of the AFM tip was 'collected'

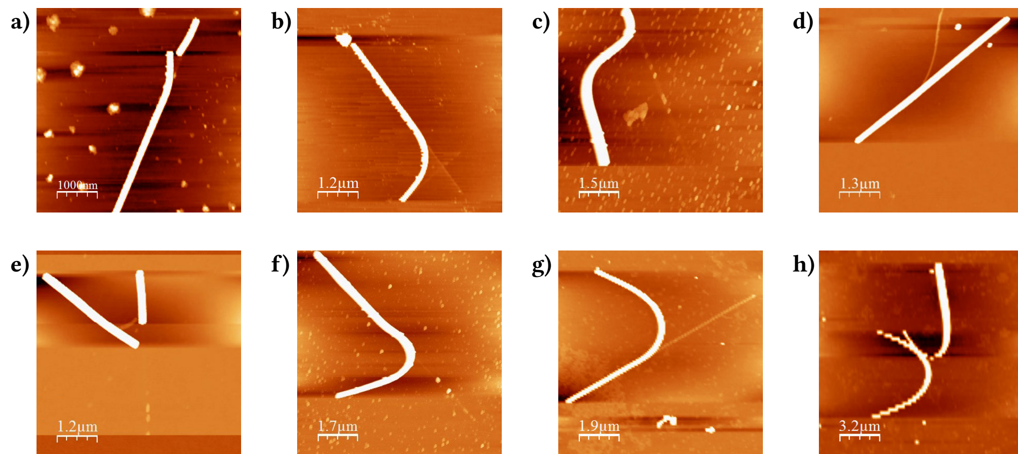

Figure 2.3. Examples of AFM manipulation on nanowires: **a)** Cutting a Nanowire. **b)** Bending a Nanowire. **c)** Flexible Nanowire. **d)** Snapping Back. **e)** Breaking after enormous Bend. **f)** Perfectly Bended Nanowire. **g)** Nanowire bended on TEM Grid. **h)** Also on a TEM grid: Using one NW as a barrier while bending another one.

during the movement. Finally a third attempt to bend the wire further, broke it as seen in figure A.4d.

Strong Strain in the Crystal Structure - Breaking after enormous Bend. The stongest bend observed i.e. the bend with the largest curvature was observed in figure 2.3e. An initial bend resulted in a turning point far from the end of the wire (fig.A.5b), while a second bend broke the wire. Figure 2.3e contains information about the bend before the NW broke, the curvature of the observed trace is the largest observed during this study and the radius of a manually fitted circle is approximated to 0.8 µm.

Perfectly Bended Nanowire. After showing how nanowires often behave while bending them, figure 2.3f shows a wire where bending was a great success. A twofold bending process resulted in a wire with a strong bend while it was large enough for device fabrication. The radius of the curvature is approximated to 0.95 µm.

Bending Nanowires on TEM Grids. Nanowires have a weaker surface interaction on the silicon nitride TEM grid compared to silicon oxide wafers, thus the result of manipulation with the AFM is different as well.

Figure 2.3g shows a NW which later was studied using High Resolution TEM and Raman spectroscopy. To achieve this bend the wire had to be pushed five times for the final image.

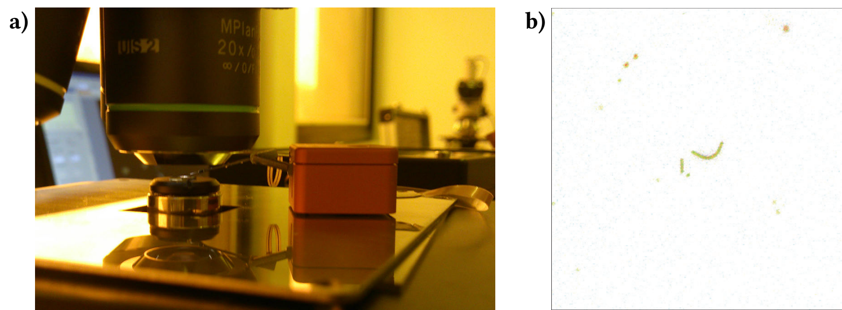

Figure 2.4. a) miBot Setup used to bend a nanowire and **b)** the final cut and bent wire (inverted image).

First observations of a NW freely moving along the surface, lead to an small experiment; It was tried to use one NW as a barrier while pushing another one against it. This was sucessfull and is shown in figure 2.3h. Further attempts to bend the lower wire in figure 2.3h broke it (fig.A.8d). The process is shown in appendix (A) in more detail.

2.2.4 The Quick and Dirty Option

During the final stage of this project, the group had a visit by Romain Tanzer, from Imina Technologies[4], presenting their nanomanipulators. The robots (miBots) use a piezo stick-slip mechanism to move freely along the surface while achieving nanometer precise positioning. They were equipped with a manipulator needle (tip diameter: 500 nm) and placed at an optical microscope. Figure 2.4a pictures the simple setup.

The miBots are controlled intuitively by a gamepad controller and a quick test showed that it was possible to cut a NW, leaving one side bended, in less than 5 minutes, while it usually takes 30 minutes or longer with an AFM. An inverted darkfield image of the bended NW is shown in figure 2.4b. No further investigations have been undertaken to verify if the NW is damaged or not.

This unexpected input to the project revealed a fast and easy, but in this situation rather uncontrolled, method to bend nanowires or do other kinds of nanomanipulation.

2.3 Strain and Defect Analysis using TEM

2.3.1 Characterization by regular TEM

Transmission Electron Microscopy was used to analyze the bended nanowires for defects and to measure the strain along the wire. First analysis using an in-house TEM

[4]Imina Technologies: www.imina.ch

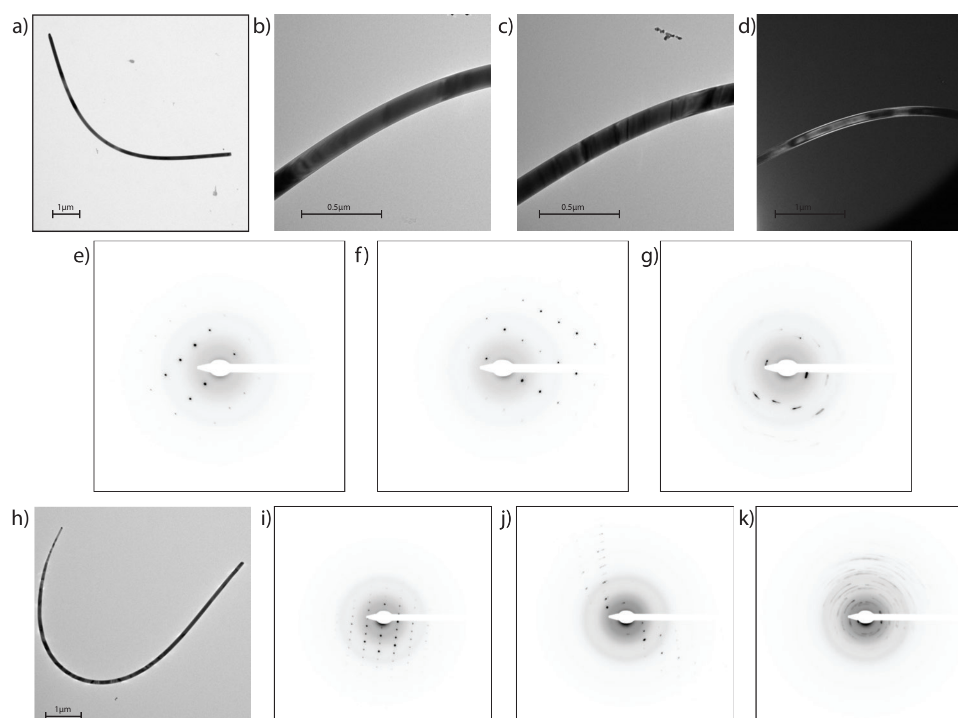

Figure 2.5. Transmission electron microscope images on two nanowires:**[SiN_NW4] (a-g):** Overview **a)** and magnified images at the bend showing shaded areas following the NW **b)** and changing during a tilt of 16 ° **c)** emphasized by a darkfield image **d)**. **e,f)** SAD patterns show rotation of the crystal structure by 104 ° which is comparable to the strength of the bend. Diffraction at the bended part **k)** showing a superposition of many slightly rotated planes. **[SiN_NW4]: (h-k)** Overview **h)** and SAD patterns **i,j,k)** of a bended wire showing the same features. Diffraction images are inverted for visibility in print.

were done together with Morten Hannibal Madsen[3] on three NWs suspended on a 50 nm silicon nitride membrane.

Images taken with the TEM include overview images of two nanowires, high magnifications of the strained part of one wire as well as selected area diffraction (SAD) patterns of strained and straight parts of the wire. The first NW is only slightly bended, as seen in figure 2.5a, magnifications of the strained part are shown in figures 2.5b and 2.5c (same spot tilted by 16 °). Clearly seen is the shading of the wire which changes along it, after rotation the shading changed completely which indicates a change in the lattice structure due to strain. Also defects and stacking faults in the wire are usually seen as spots or sharp lines perpendicular to the wire direction. The dark field image in figure 2.5d emphasizes the picture of pure crystalline nanowires further. Diffraction patterns of the top, bottom and bended part are seen in figures 2.5e,f,g respectively. The

clearly defined spots resulting from diffraction at the straight parts reveal pure crystal structures; the diffraction patterns are rotated in respect to eachother with an angle of 104 °, which is in excellent agreement with the angle between the two straight parts of the wire. The third diffraction image (fig.2.5g) shows a superposition of many slightly rotated crystal planes, as expected in a bended crystal. The angle corresponding to the rotation is measured to 13 ° which should be comparable to the strain visible in the SAD-area. Diffraction patterns for the other NW (fig.2.5h) are shown in figures 2.5i,j,k. The wire is bended by a larger angle which is reflected in the diffraction patterns as well, the pattern rotation here is 165 ° and comparable to the overview image as well. The upper end of the wire is not totally straight which is the cause for the slight rotation in the respective diffraction pattern. A strong rotation of 44 ° is seen at the bended part, the increase in comparison to the first wire could be a consequence of a larger curvatrue, but more likely this is due to the SAD configuration which might cover a larger part of the wire and thereby include diffraction from a broader range.

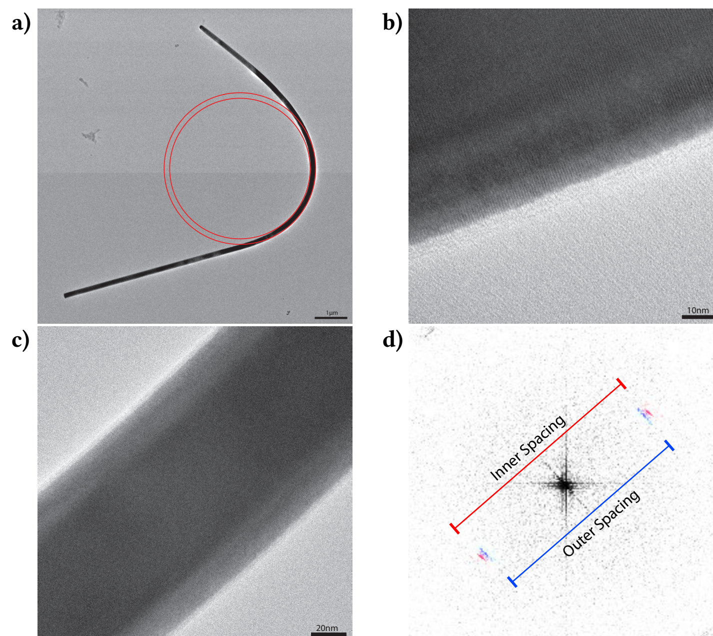

Figure 2.6. **[SiN_NW2]** HRTEM images showing a bended nanowire **a)** and magnifications at the bended part **b,c)** as well as the result of a FFT **d)** taken on **c)** which shows the increased lattice spacing across the wire.

2.3.2 HRTEM characterization at Risø

During the project there was an opputurnity to use a HRTEM placed at Risø, here images were taken together with Morten Hannibal Madsen[3] and Erik Johnson[5].

One NW was analyzed with the HRTEM, images are collected in figure 2.6. Full sized images are printed in appendix B. An overview image (fig.2.6a) shows the bended nanowire and a circle manually fitted to the bended part, which has a radius of 2.2 µm. Several images like figure 2.6b were taken along the inside and the outside of the wire, at the straight ends as well as the bended part; They show single layers of the crystal structure. These pictures clearly show that bending the wires does not induce defects. This statement is emphasized by comparison of the radii of the circles in figure 2.6a to the change in lattice spacing from the inner and the outer part of the wire. The change in lattice spacing was derived by a fast fourier analysis on the image shown in figure 2.6c. Comparing the result (2.6d) the outer spacing is about 5.1 % larger (real space) which compares well with the increased radius of the circle which is close to 6.4 %.

2.4 Raman Spectroscopy

Raman spectroscopy was conducted on 5 bended nanowires, two of them suspended on the 50 nm silicon nitride TEM grid while the others were bended on the silicon oxide samples.

2.4.1 Spectra along Bended Nanowires

First Raman measurements on a bended wire were conducted with the APD, measuring photons with wavelengths ranging from 517 nm to 560 nm. A topological image, such as in figure 2.7a, was created by measuring the intensity (i.e. counting photons) of the Raman signal in an array covering $100\,\mu m^2$. Photon counts ranged from ≈ 10 in the background to ≈ 100 at the wire which is clearly distinguished from the background.

Whole spectra centered along the wire were taken using the CCD-Detector, an integration time of 60 s resulted in spectra as shown in figure 2.7b. The spectra were analyzed by fitting Lorentzian functions to the normalized transversal optical (TO) peaks around $215\,cm^{-1}$, the result of the fitting procedure is shown in figure 2.7c. A Raman shift of $\approx 215.3\,cm^{-1}$ is observed in the straight parts while it is about $0.3\,cm^{-1}$ lower in the bended region of the wire, which is less than the resolution of the CCD detector / grating configuration of $1.5\,cm^{-1}$. The width of the peaks increases for the second and the third spectra at the bended region.

This data shows a general trend of decreasing Raman shift as well as an increased width of the main peak arising from the InAs nanowire. The broader peaks at the bended regions are expected as the strained NW will have vibrational modes related to the lattice spacing. As determined by TEM, a change in the lattice structure is observed,

[5] Niels Bohr Institue, University of Copenhagen

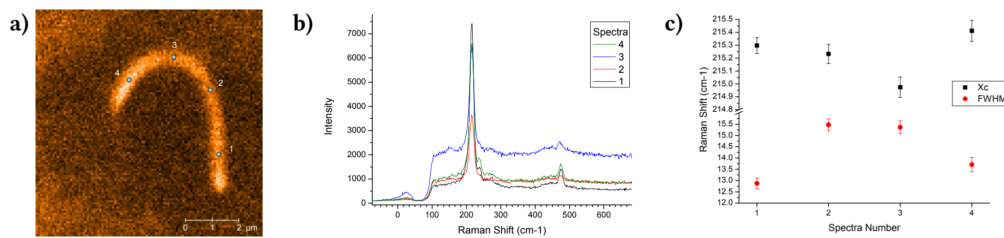

Figure 2.7. [SiN_NW3]: a) Topographical Raman image aquired using an APD and a bandpass filter (range: 215 -260 nm. **b)** Spectra aquired at the points indicated in **a)**. The main peak is analyzed and peak position as well as FWHM is shown in **c)**

vibrational modes will change in energies accordingly and overlap in the respective spectra.

During detailed measurements, as described in section 2.4.2, polarization effects were observed and thus studied further by increasing the number of single spectra taken along the wire as well as an increased integration time at the detector.

The setup used during the measurements did not enable for control or measurements of the the laser polarization, thus the sample was rotated by 90 ° between two detailed measurements to reveal some information. Unfortunately a bug in the acquisition software, which still is in development, resulted in loss of data for one set of measurements. Only screenshots exist but no statistics could be executed on the respective spectra.

One set of measurements is presented in figure 2.8, again showing an overview of the NW generated using the APD (fig. 2.8a) with increased acquisition time per pixel resulting in a larger contrast. 14 spectra were taken as indicated, and plotted in figrue 2.8b (normalized) with an offset for comparison. Acquisition time of the CCD was increased to 2 min for a better signal to noise ratio and to allow for studies on the longitudinal optical (LO) (side)peak accompaining the main TO peak.

Results of Lorentzian linefits are shown for the main and side peaks in figures 2.8c and 2.8d. By comparison of linespectra taken before and after rotation of the sample it was observed that the LO peak changed intensity due to polarization i.e. the side peak was largest right at the bend and only slightly visible at the ends of the wire. A positional difference after rotation could not be observed due to the lack of data.

Interestingly the position of the main peak is roughly constant before and after the abrupt change between spectra no.9 and 10. which is not yet understood. The increased width of the main peak at the bend however compares well to the first measurement (fig.2.7c) as well as it was reported in [7] for InP nanowires. The side peaks also seem to have a decreased Raman shift and an increased width at the bend but as the peak is not strong enough in spectra 6,7 and 8 this is only a vauge observation.

The inset in figure 2.8a shows the topographical image of the rotated wire, the bright parts correspond roughly to intense sidepeaks in the spectra, comparing the bended part of the two images clearly show a polarization effect.

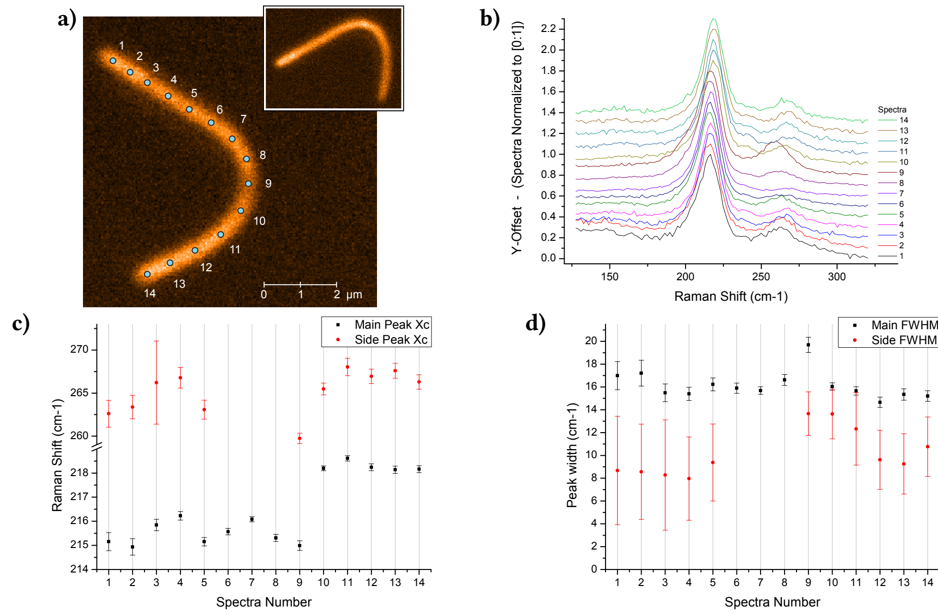

Figure 2.8. [SiN_NW2]: a) Topographical Raman images (inset rotated by 90 ° to show polarization effect). **b)** Spectra taken at the indicated points. Main and side paks are analyzed as shown in Topographical Raman image and **d)**.

2.4.2 Mapped Raman Spectra

Topographical Raman images, as shown in the previous section, do not allow dynamic investigation of samples. New spectra have to be acquired manually at desired locations of a sample. This might be inconvinient for a sophisticated analysis of samples like the bended wires in this study. To eliminate this limitation the group of Tom Vosch[2] implemented an updated software to the system which was just installed when this data was aquired. Instead of counting photons (with the APD) of the Raman signal at every position of the sample, the updated software used the CCD detector to aquire real spectra at those points to create a map of Raman spectra. This allows for dynamic studies of Raman signals at different energies, while the full range of the spectra still is available.

As the acquisition software still is in development, data analysis is currently only based on the raw spectra taken. The benefits of true mapped spectra is the broad range of the spectra, which calls for a a dynamic data inspection. Thus a program was developed during the project to allow for this. Figure 2.9a shows a screenshot of the developed "Raman Light Viewer", currently the program is capable of reading mapped spectra, calibrating the data to a reference spectra and displaying the intensity of the spectra narrowed by a 'bandpass' filter as an image. It also allows for a dynamic inspection of single spectra, selectable in the mapped image as well as exporting those

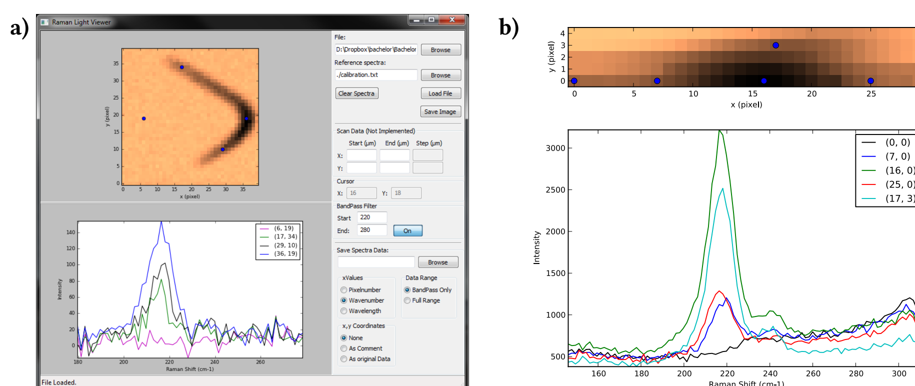

Figure 2.9. a) Screenshot of the "Raman Light Viewer" which was developed to dynamically analyze Raman data and an example output **b)**.

selected spectra and the currently shown plots. An example of the graphical output is seen in figrue 2.9b.

In general, spectra mapping is a time intense process as every spectra requires acquisition times of 30 s and above. During long acquisition processes (1 h and above) movement of the sample or a slight defocusing was observed. Figure 2.9b is an example of defocusing during acquisition. The intention of this measurement was to measure spectra across the wire at the most bended part, which was achieved by 5 linescans spaced by 100 nm in the y direction. Every spectra here is an integration of 60 s (2.5 h in total).

Linescans at straight and bended parts of the wires have been analyzed the corresponding data of such linescans is shown in figure 2.10. Peak positions (fig.2.10a,c) and the corresponding FWHM (fig.2.10b,d) at a unstrained and right at a bended part of a wire were extracted.

The Raman spectra only corresponds to a slight part of the wire, which in turn does show a changed lattice spacing across it, as analyzed with TEM. Thus it was expected that the innermost and outermost spectra at the bended part of the wire would differ significantly. The data (fig. 2.10b,2.10d) however does not show a clear change of the spectra in these areas, it is rather consistent. Even comparison of the bended and the straight part does not show a clear distinction.

The trend of a decreasing Raman shift at both the straight and the bended part is noted and is expected to be a temperature dependent change in the Raman signal, arising from heating by the laser. This is reasonable due to the fact that the silicon peak does not show this behavior (not shown). However, further studies are required to verify this.

It was shown by Hormann et al.[15] that there is a strong polarization effect on InAs nanowires. It is claimed that polarization only affects the main peak position. This is in agreement with the observation done here, where the positional change of the side peak

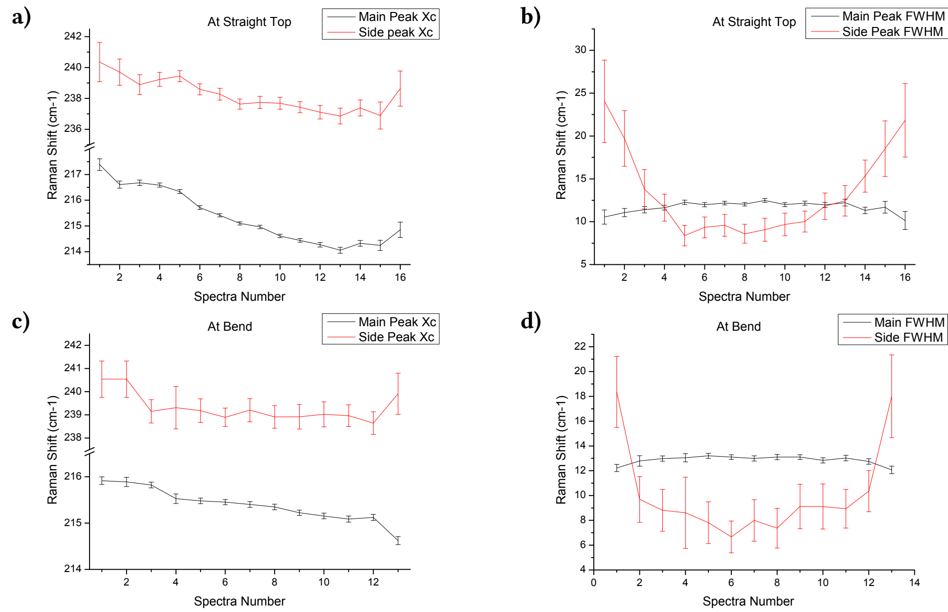

Figure 2.10. Analysis of linespectra across a nanowire at a straight and a bended part, main and side peak positions and respective FWHM are shown.

is expected to arise from the induced strain. However, also sample degradation would affect on the Raman signal, it is an important step, before further studies are conducted, to veryfy that the crystal structure remains intact after intens raman measurements.

Since this data was aquired the setup was equipped with a controllable polarizer which allows for sophisticated analysis of the polarization effect as well as a distinction to effects induced by strain.

2.4.3 Possible Setup Improvements

To implement Raman spectroscopy as a general characterization tool for small nanostructures, improvements are necessary. Improvement of the setup could include but is not limited to the following.

1. Verifying the temperature dependence is a requirement for all further studies. If there is a depencence, maintaining a constant temperature is required for linespectra, where the laser only moves by a few nanometers, also pauses between linespectra could reduce a dependence. Low temperature measurements would be optimal to further limit thermally excited vibrations in the crystal and thus impruve the signal to noise ratio.
2. A combination of topographical Raman spectra, acquired with the APD, and mapped spectra, acquired with the CCD-detector, could improve aquisition times. As for now

detailed spectra are taken for the whole area imaged, masking areas of interest would thus reduce the number of spectra recorded.

3. A CCD-detector with a highly increased sensitivity would allow for fast spectra recording, which again limits the total aqusition time and reduces generation of unusable data by sample-movements.

2.5 Device Fabrication for Electron Transport Measurements

For electron transport measurements on nanowires it is nessecary to contact them with metallic leads. As this is a standard technique, recepies from the group were adapted for e-beam lithography. This includes spincoating the chips with a copolymer[6] and polymethyl methacrylate[6] (PMMA) stack, which was observed to relax bended nanowires. Furthermore it was observed that washing, heating (185 ℃), schocking (dropping) and storing (2 weeks) samples with bended wires resulted in relaxation of the bend. Thus a 5 nm layer of Al_2O_3 was deposited on samples which were to be used for device fabrication. Deposition was conducted by atomic layer deposition (ALD) without heating the ALD chamber, which typically had a temperature around 60 ℃.

Then a typical procedure for e-beam lithography was conducted as shown in figure 2.11, where the sample is covered by ≈100 nm copolymer and ≈200 nm PMMA by

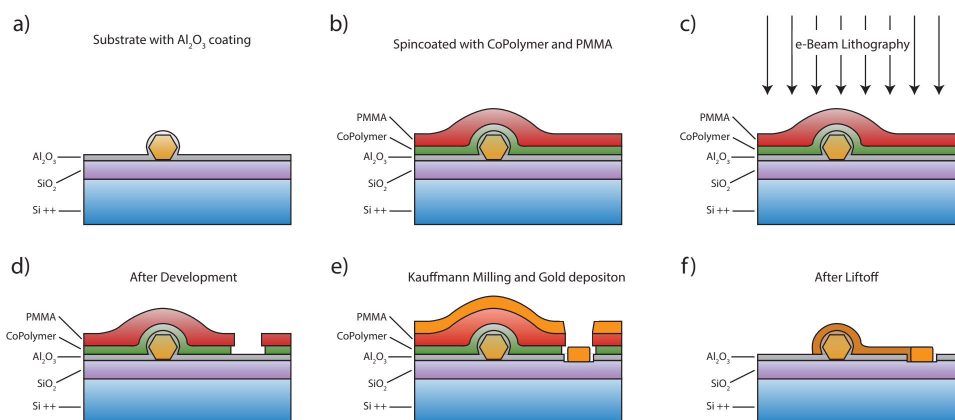

Figure 2.11. Device fabrication process: **a)** 5 nm Al_2O_3 cover to hold nanowires in place. **b)** Spin-coating of CoPolymer and PMMA. **c)** e-beam lithograpy. **d)** Development. **e)** Kaufmann milling to remove the Aluminium and natural oxide layer on the NW and Ti/Au deposition. **f)** After liftoff only the contacts remain.

[6]MicroChem: www.microchem.com

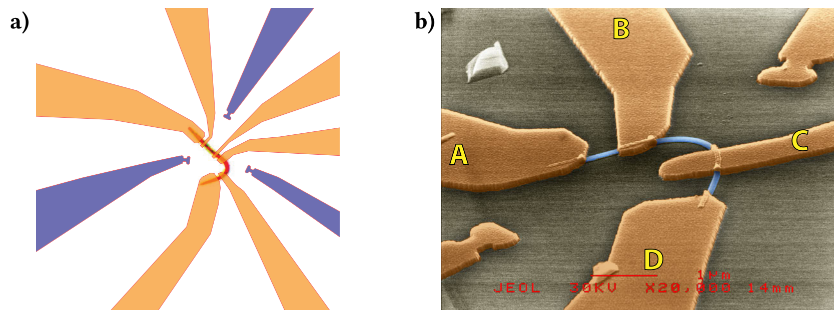

Figure 2.12. **a)** A design of a device which allows for 4-point measurements on strained and straight segments of a nanowire and **b)** a device on a smaller wire contacted by e-beam lithography.

spincoating at 4000 rpm for 45 s (fig.2.11b). Lithography uses a focused e-beam to expose the resist as defined by the device design (fig.2.11c). The copolymer and PMMA differ in e-beam sensitivity thus more copolymer is removed during development in PG-Remover[6] which results in an undercut as shown in figure 2.11d. After development the aluminum oxide and the natural oxide layer on the NW were removed by ion milling. A Kaufmann source sputters neutralized Argon ions on the surface to "kick out" atoms on the surface. The whole sample is then covered with a 5 nm Ti sticking layer and a 100 nm Au layer which is used for the electrical contacts (fig.2.11e). The resist is then dissolved in PG-remover which lifts the metal sheets from the unexposed areas of the sample, leaving the desired leads behind. Devices were designed to allow 4-point measurements on straight and bended segments of the NWs, an example design is shown in figure 2.12a, where the orange leads have ohmic contact to the wire.

To suppress electron transport and to control the position of 'transport channels' sidegates were planned. To achieve small distances between the wire and the desired sidegates the exact position of the wire in respect to the contacts is needed. Thus a second lithographic step is needed after determining the position with the AFM or SEM which will allow gate-wire distances below 100 nm. The blue contacts shown are preparations for those sidegates.

During the project, the first step was achieved, a bended wire was contacted with Ti/Au leads as seen on the SEM image in figure 2.12b. The wire was too short to allow for 4-point measurements on the straight and bended segments thus the design was altered.

2.6 First Electron Transport Measurements

Electronic measurements were performed on the device shown in figure 2.12b in a probe station at room temperature in vacuum.

The probe station is commonly used to verify ohmic contact to nanowires before conducting low temperatue measurements. Here a first measurement between the outermost contacts A and D (fig.2.12b) revealed a gate dependent resistance ranging from $13.7\,\mathrm{k\Omega}$ at a backgate voltage ($\mathrm{V_{BG}}$) of $+10\,\mathrm{V}$ to $52.2\,\mathrm{k\Omega}$ at $-210\,\mathrm{V_{BG}}$ (fig.2.13a). These measurements were performed at a source drain voltage of $V_{SD} = 2\,\mathrm{mV}$ between contacts A and D. The highly doped silicon wafer is contacted to the probe station with conducting carbon-tape to act as a backgate.

The backgate voltage is usually not tuned that far, here this was done because the source-drain current I_{SD} could not be turned off which is an expected feature of semiconductors. Also back gate leackage current stayed below 200 pA during this measurement, indicating bad contact or great quality of the insulating silicon oxide layer.

Further measurement were conducted a week later to verify ohmic contact for all leads. This measurement revealed contact resistances ranging from $10.8\,\mathrm{k\Omega}$ to $34.9\,\mathrm{k\Omega}$ all at $\mathrm{V_{BG}} = 0\,\mathrm{V}$. Also a typical hysteresis effect was observed in all measurements by tuning $\mathrm{V_{BG}}$ from -10 V to +10 V ($V_{SD} = 2\,\mathrm{mV}$) which is shown in figure 2.13b.

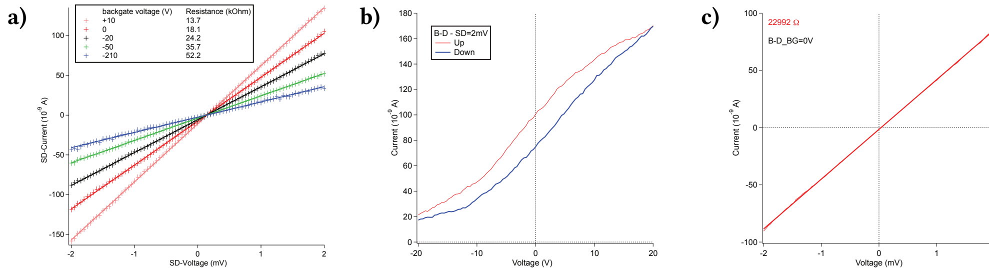

Figure 2.13. First electronic measurements show **a)** gate dependent resistance measurements with bad contact to the backgate, **b)** hysteresis effect while tuning V_{BG} from -10 V to +10 V at $V_{SD} = 2\,\mathrm{mV}$ and **c)** Ohmic contact was achieved.

3 Conclusion and Outlook

3.1 Conclusion

Precise and coherent manipulation of nanostructures is still a challenge these days, this thesis presents a thoroug analysis of nanomanipulation based on single crystal nanowires.

Strain was induced in single nanowires using an Atomic Force Microscope (AFM), they were bended and an optimization of the bending procedure was conducted. It is shown that using this optimized procedure, allows for fast and precise control of manipulation with an AFM, which simultanously can be used for detailed analysis of the investigated nanostructures.

Furthermore bended nanowires were analyzed by Transmission Electron Microscopy (TEM). It is verified that manipulating nanowires physically by an AFM tip does not harm the crystal upon impact. Also the crystal structure remains intact in the strained nanowires. As verified by High-Resolution TEM, crystal planes strained along the wire axis are perfectly aligned.

Raman spectroscopy was performed to implement non invasive strain analysis, eliminating the need of TEM compatible samples. Measurements in the diffraction limit reveal a strain dependent Raman shift along the wire. Detailed measurements were conducted to gain deeper knowledge of the crystal structure within the strained wires. However, the information acquired is limited due to setup limitations.

Finally a proof of principle is given for fabrication of electronic devices to allow for further low temperature measurements to gain knowledge about stress effects on electron transport in this mesoscopic regime.

3.2 Outlook

This study answers some questions, related to strain induced by nanomanipulation, while it leaves room for further studies. As a bachelors project is limited in time further studies will be conducted in a following project.

While Raman spectroscopy leaves room for improvement through setup changes, electronic measurements at cryogenic temperatures will reveal knowledge on strain induced changes on quantized electron transport.

Acknowledgements

Foremost I would like to thank my great friend, Nino Ziino, contributing with time for discussions, help in the lab and generally good times during the whole process of this project.

Also I would like to thank my supervisor, Thomas Sand Jespersen, for inspiration and making all parts of this project possible. Further thanks to Erik Johnson and Morten Hannibal, taking me to Risø was a great experience. I'd also like thank Tom Vosch for his help and trust during an intense time with Raman spectroscopy.

Finally thanks to all members in the QDev group for their help in all phases of this project, especially sharing time on a cup of coffee.

Bibliography

[1] E. C. Garnett et al. *Nanowire Solar Cells*. In: *Annual Review of Materials Research, Vol 41* 41 (2011), pp. 269–295.

[2] K. L. Martinez et al. *Intact Mammalian Cell Function on Semiconductor Nanowire Arrays: New Perspectives for Cell-Based Biosensing*. In: *Small* 7.5 (2011), pp. 640–647.

[3] S. A. Dayeh. *Electron transport in indium arsenide nanowires*. In: *Semiconductor Science and Technology* 25.2 (2010).

[4] Morten Hannibal Madsen. "Indium Arsenide Nanowires Fabrication, Characterization and Biological Applications". PhD thesis. 2012.

[5] K. Flensberg and C. M. Marcus. *Bends in nanotubes allow electric spin control and coupling*. In: *Physical Review B* 81.19 (2010).

[6] C. Y. P. Chao and S. L. Chuang. *Spin-Orbit-Coupling Effects on the Valence-Band Structure of Strained Semiconductor Quantum-Wells*. In: *Physical Review B* 46.7 (1992), pp. 4110–4122.

[7] J. N. Chen et al. *Probing Strain in Bent Semiconductor Nanowires with Raman Spectroscopy*. In: *Nano Letters* 10.4 (2010), pp. 1280–1286.

[8] T. Junno et al. *Controlled Manipulation of Nanoparticles with an Atomic-Force Microscope*. In: *Applied Physics Letters* 66.26 (1995), pp. 3627–3629.

[9] D. Fotiadis et al. *Imaging and manipulation of biological structures with the AFM*. In: *Micron* 33.4 (2002), pp. 385–397.

[10] M. Bordag et al. *Shear stress measurements on InAs nanowires by AFM manipulation*. In: *Small* 3.8 (2007), pp. 1398–1401.

[11] Bruce Alberts et al. *Molecular Biology of The Cell*. 5th ed. Garland Science, 2008.

[12] ETH Zürich. *Imaging and Diffraction in the TEM (schematic)*. URL: http://www.microscopy.ethz.ch/TEMED.htm.

[13] W. H. Weber and R. Merlin. *Raman Scattering in Materials Science*. Materials Science. Springer, 2000.

[14] Hannibal Morten. *InAs Nanowire Catalog*. URL: https://wiki.nbi.ku.dk/w/qdevwiki/img_auth.php/9/9b/GrowthCatalog20101026-small.pdf.

[15] N. G. Hormann et al. *Effects of stacking variations on the lattice dynamics of InAs nanowires*. In: *Physical Review B* 84.15 (2011).

Appendix

A Bending Nanoowires using an Atomic Force Microsope

Figure A.1. [D01_NW03] - Cutting a Nanowire. Cutting a nanowire, resulting from a high tip velocity of 2 µm/s.

Figure A.2. [D01_NW02] - Bending a Nanowire. Bending a NW at the lower end wit a single *x*-*y* movement obtaining a bend of 75 °.

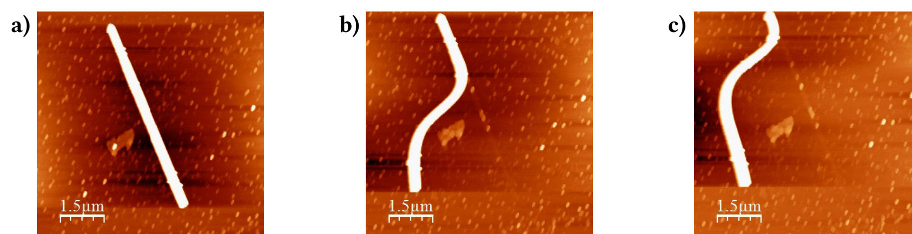

Figure A.3. [D02_NW03] - Flexible Nanowires. The most flexible nanowire observed. Pushed to the wire three times without breaking.

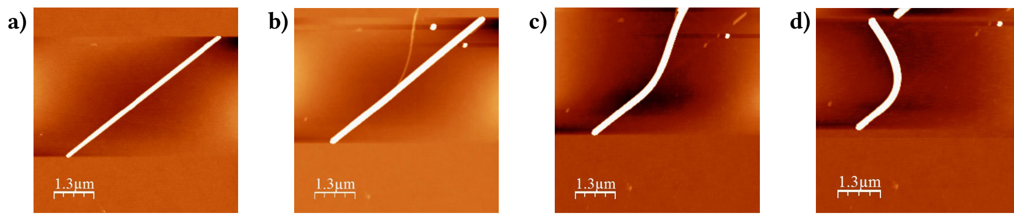

Figure A.4. [D09_NW01] - Strong Strain in the Crystal Structure - Snap Back A nanowire snapped back after a first push.

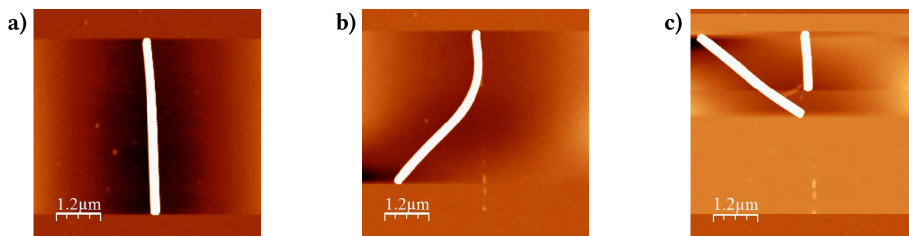

Figure A.5. [D09_NW03] - Strong Strain in the Crystal Structure - Breaking after enormous Bend. Broken NW leaving a trace of the strongest observed bend.

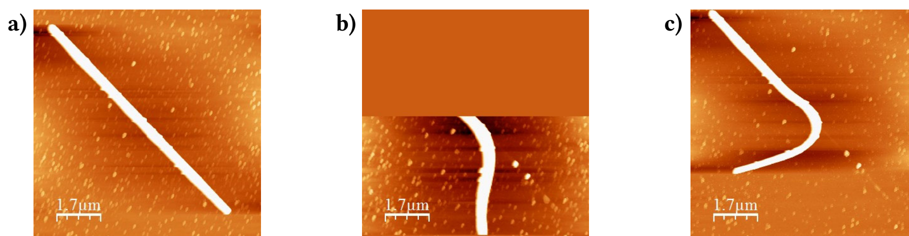

Figure A.6. [D09_NW04] - Perfectly Bended Nanowire. Perfectly bended nanowire fullfills all criteria for device fabrication.

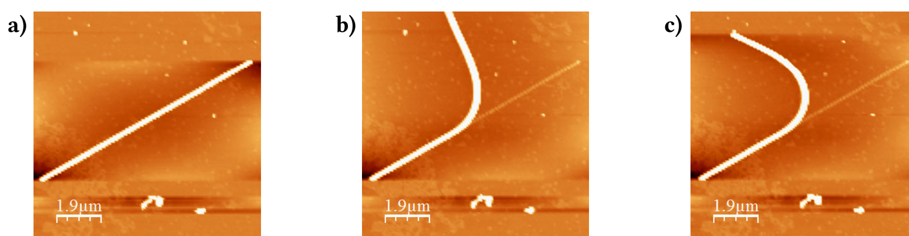

Figure A.7. [SiN_NW2] - Bending Nanowires on TEM Grids Nanowire bended on a 50 nm silicon nitride membrane.

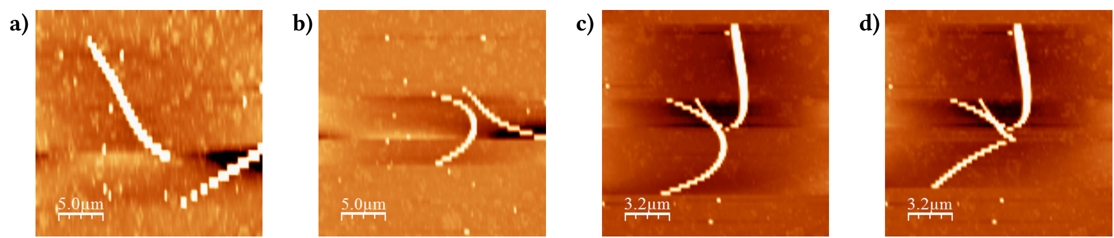

Figure A.8. [SiN_NW5] - Bending Nanowires on TEM Grids. Two NWs were pushed along the surface against eachoter.

B High Resolution TEM Images

Here some HRTEM images are shown to emphasize the atomic planes visible.

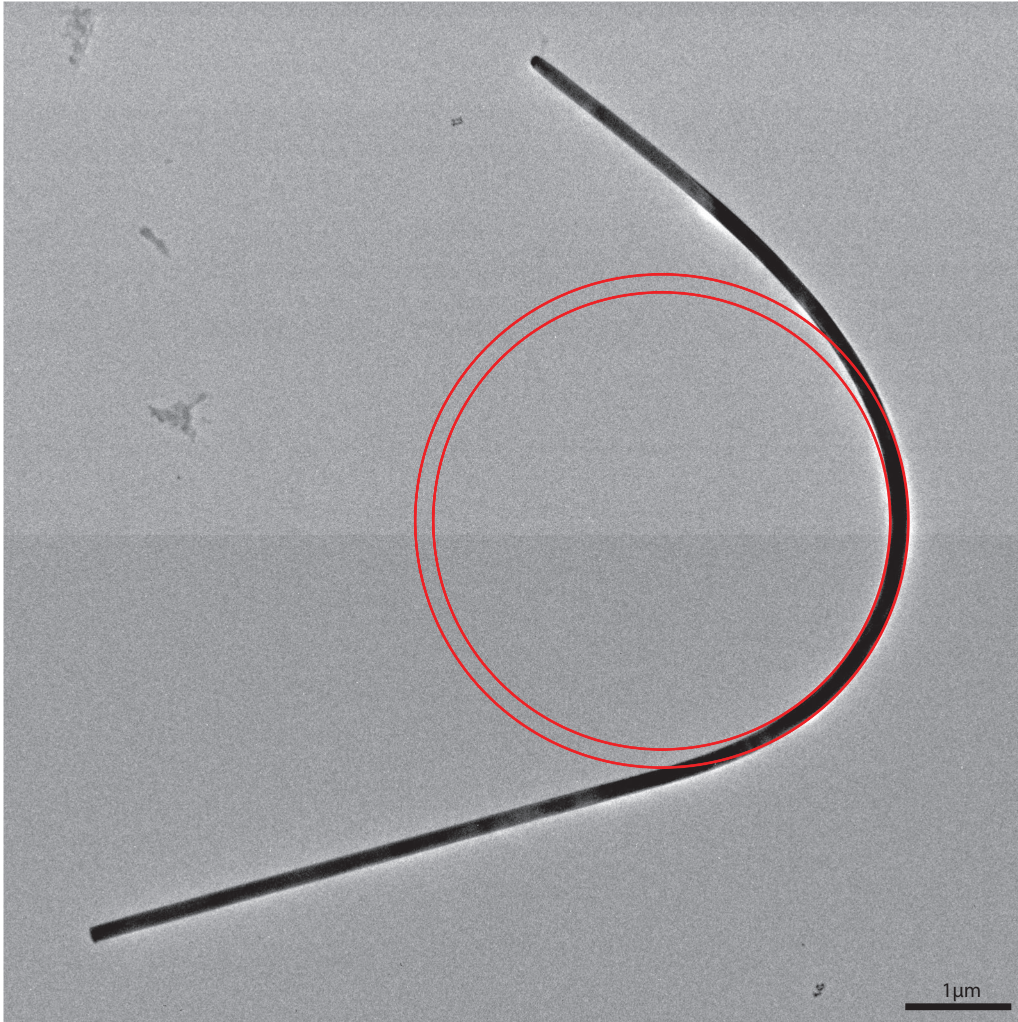

Figure B.1. [SiN_NW2] HRTEM images showing a bended nanowire, a circle is manually fitted to estimate the radius of curvature at the bended part.

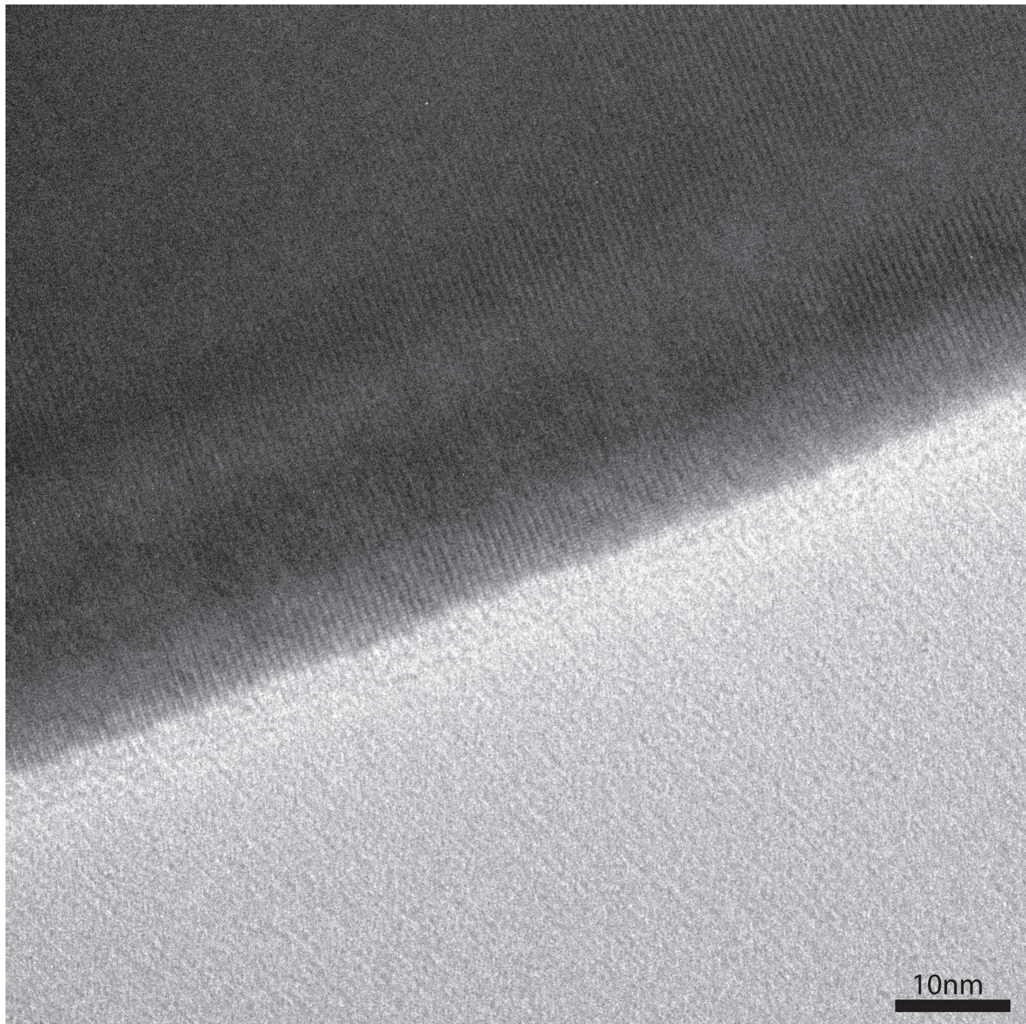

Figure B.2. [SiN_NW2] A magnifications at the outer side of the bended part (500kx).

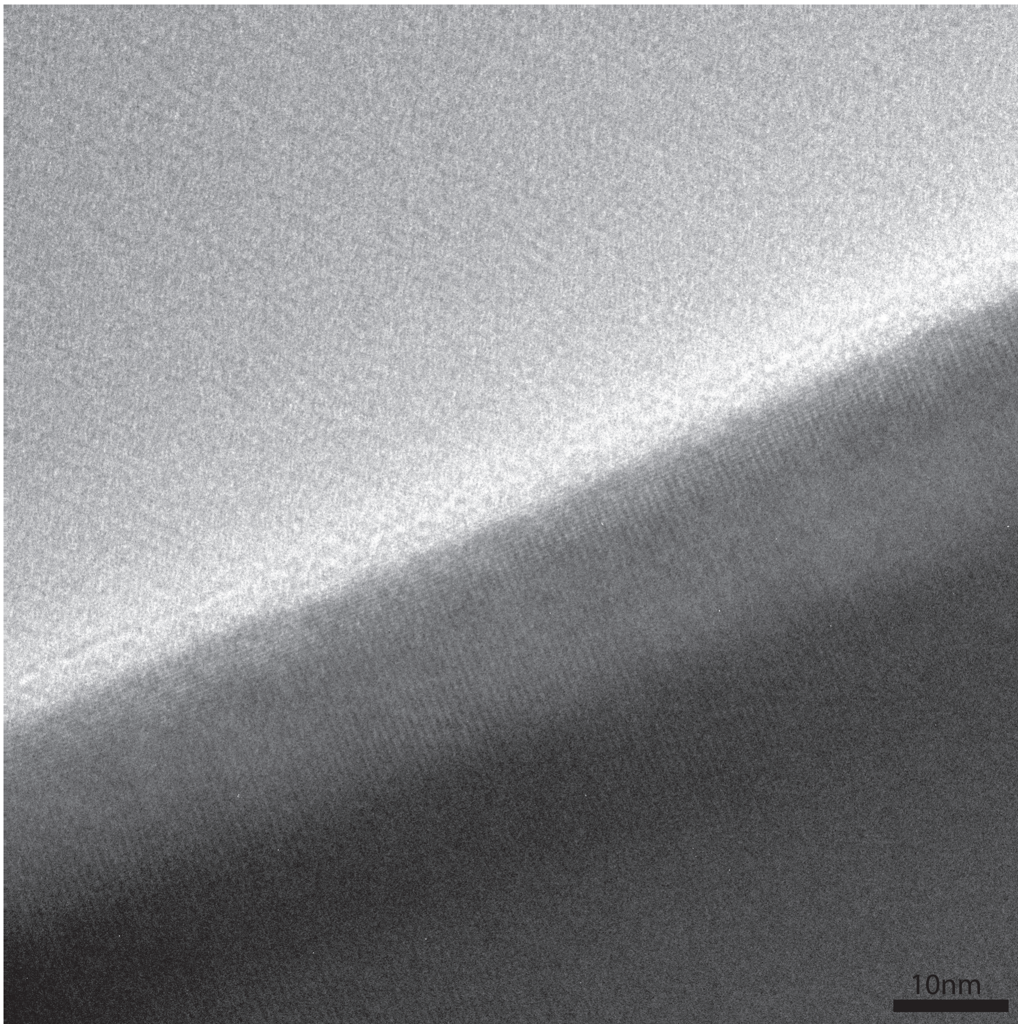

Figure B.3. [SiN_NW2] A magnifications at the inner side of the bended part (500kx).

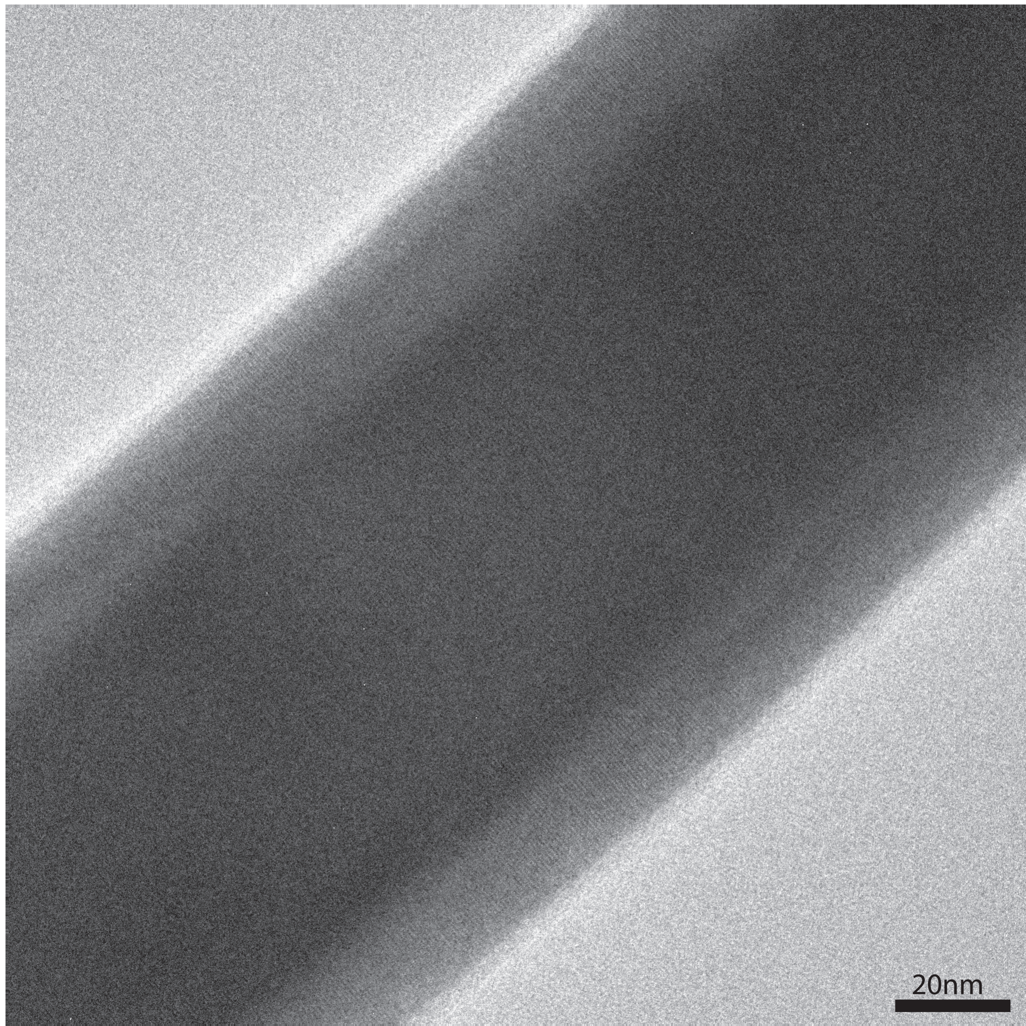

Figure B.4. [SiN_NW2] A magnification of 250kx used for FFT analysis.

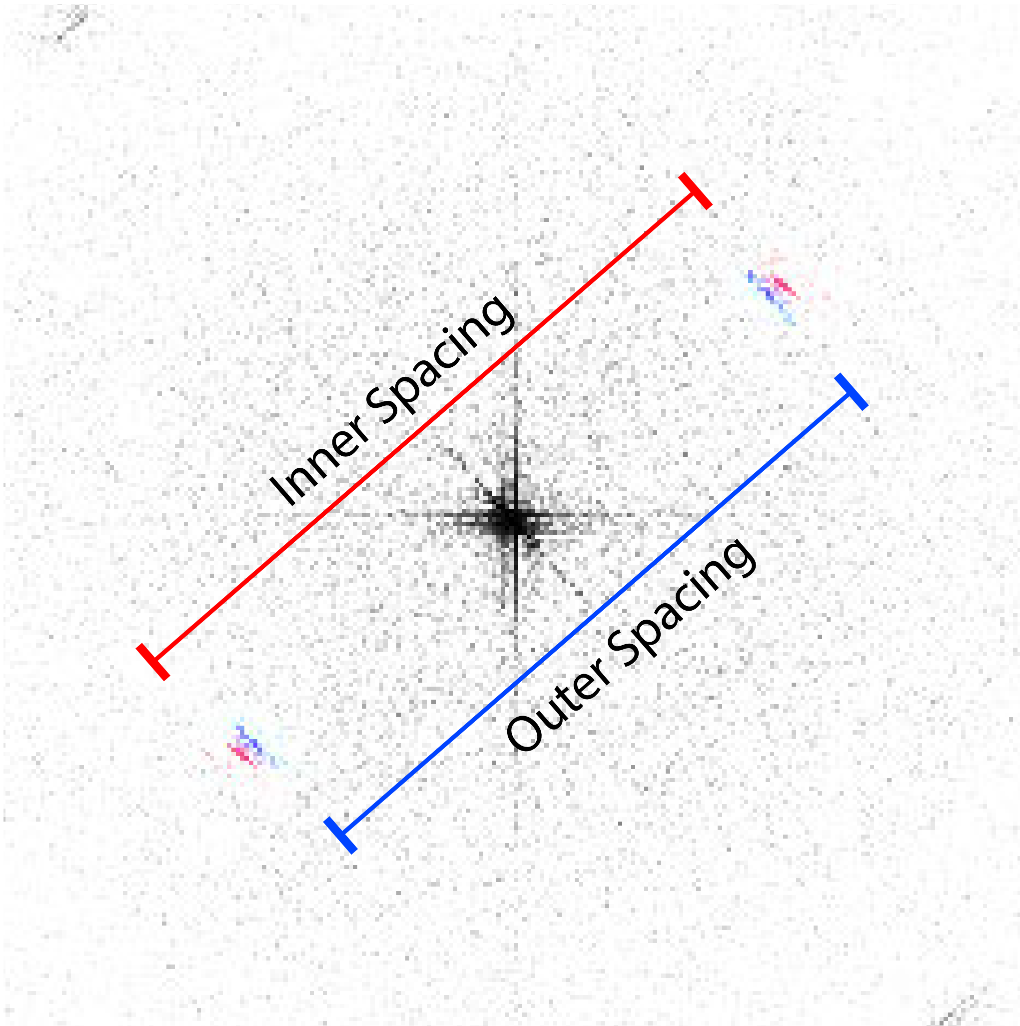

Figure B.5. [SiN_NW2] FFT analysis shows an increased lattice spacing across the wire.